Light Trapping Textures Designed by Electromagnetic Optimization for Subwavelength Thick Solar Cells

Vidya Ganapati, Owen D. Miller, and Eli Yablonovitch

***Abstract*—Light trapping in solar cells allows for increased current and voltage, as well as reduced materials cost. It is known that in geometrical optics, a maximum $4n^2$ absorption enhancement factor can be achieved by randomly texturing the surface of the solar cell, where n is the material refractive index. This ray-optics absorption enhancement (AE) limit only holds when the thickness of the solar cell is much greater than the optical wavelength. In subwavelength thin films, the fundamental questions remain unanswered: 1) what is the subwavelength AE limit and 2) what surface texture realizes this optimal AE? We turn to computational electromagnetic optimization in order to design nanoscale textures for light trapping in subwavelength thin films. For high-index thin films, in the weakly absorbing limit, our optimized surface textures yield an angle- and frequency-averaged enhancement factor $\sim$39. They perform roughly 30% better than randomly textured structures, but they fall short of the ray optics enhancement limit of $4n^2 \sim 50$.**

***Index Terms*—Light trapping, optimization, subwavelength.**

I. Introduction

TEXTURING of solar cell surfaces allows for absorption enhancement, owing to the coupling of incident light rays to totally internally reflected modes within the cell, i.e., light trapping. It is known that in the ray-optics regime, where the thickness of the solar cell is much greater than the wavelength of light, the maximum absorption for weakly absorbed rays is given by [1]

$$A = \frac{\alpha d}{\alpha d + \frac{1}{4n^2}} \tag{1}$$

where α is the absorption coefficient, d the thickness of the material, and n the index of refraction. This maximum absorption limit assumes a perfect rear mirror. We can compare this with the single-pass absorption of the weakly absorbed light

$$A = 1 - e^{-\alpha d} \approx \alpha d. \tag{2}$$

The AE is the actual absorption divided by the single-pass absorption. The maximum AE in the ray-optics regime is, thus, given by (1) divided by (2); in the limit of a very weakly absorbing material the AE factor is given by $\mathrm{AE} = 4n^2$.

With light trapping, we can achieve high absorption, even for thin absorber layers. Short-circuit current (J_{sc}) and fill factor improvements occur due to better carrier extraction in thin layers. Additionally, open-circuit voltage (V_{oc}) improvements occur, owing to increased carrier concentration. In high quality materials, such as gallium arsenide, efficiency improvement can be substantial, due to improvement in external fluorescence yield [2], [3]. We also reduce material cost by achieving the same current in a thinner material.

In recent years, light trapping has seen renewed interest in the subwavelength regime, which is applicable to increasingly thin solar cells [4], [5]. In this regime, where the thickness of the solar cell is less than the optical wavelength, traditional ray optics does not hold, and the fundamental unanswered questions are 1) what is the upper bound on absorption enhancement, 2) and what surface texture realizes this limit?

In the subwavelength regime, there are discrete propagating modes (i.e., modes that are totally internally reflected), which can no longer be modeled as a continuum density of states. Stuart and Hall [6] attempted to establish the AE limit in the subwavelength by accounting for these discrete propagating modes, but they make the assumption that the introduced texture does not change the modal structure from that of a flat slab. This assumption does not hold, especially for thin solar cells where the amplitude of the texture is on the order of the thickness. In order to calculate a true limit in the subwavelength, the full modal structure needs to be taken into account, self-consistently. Yu *et al*. [5], [7], [8] also attempt to establish a fundamental limit in the subwavelength regime, but their approach depends on knowledge of the modal structure. In this study, we make no assumptions about the modal structure, instead numerically finding the optimal subwavelength surface texture by using computational inverse electromagnetic design.

Our work differs from prior efforts to find the optimal surface texture for thin absorber layers in the following ways:

1) Our absorber thickness is subwavelength, i.e., the wavelength of the light in the material is greater than the average thickness of the material. Many papers look at texturing

Manuscript received July 15, 2013; revised August 27, 2013; accepted August 27, 2013. Date of publication September 17, 2013; date of current version December 16, 2013. This work was supported by the DOE "Light-Material Interactions in Energy Conversion" Energy Frontier Research Center under Grant DE-SC0001293 and the National Energy Research Scientific Computing Center, which is supported by the Office of Science of the U.S. Department of Energy under Contract DE-AC02-05CH11231. The work of V. Ganapati is supported by the Department of Energy Office of Science Graduate Fellowship Program (DOE SCGF), made possible in part by the American Recovery and Reinvestment Act of 2009, administered by ORISE-ORAU under Contract DE-AC05-06OR23100.

The authors are with Material Sciences Division, Lawrence Berkeley National Laboratory, University of California, Berkeley, CA 94704, USA (e-mail: vidyag@berkeley.edu; odmiller@math.mit.edu; eliy@eecs.berkeley.edu).

Color versions of one or more of the figures in this paper are available online at http://ieeexplore.ieee.org.

Digital Object Identifier 10.1109/JPHOTOV.2013.2280340

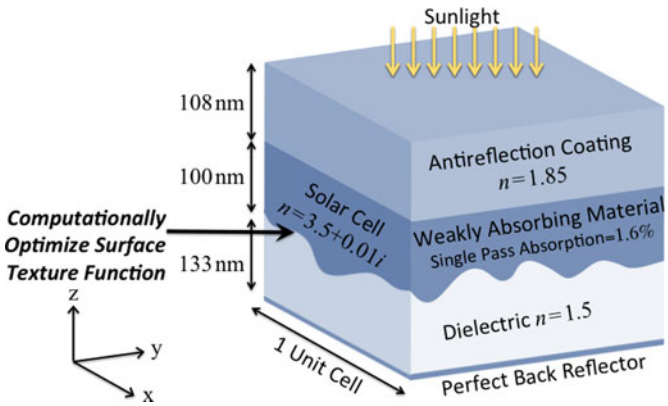

Fig. 1. The bottom surface texture of the absorbing material is computationally optimized. This diagram is a schematic of one unit cell; there are periodic boundary conditions along the *y*–*z* and *x*–*z* planes.

for absorber thicknesses in the micron range [9]–[20], a regime generally governed by ray optics.

2) To evaluate the light trapping performance of a texture for a flat-plate nonconcentrating, nontracking solar cell, we report the AE averaged over frequency and over all angles in the hemisphere. A valid comparison against the ray optics limit must be angle- and frequency-averaged, instead of over a limited angular range [9]–[11], [20]–[25] or a narrowband of frequencies [26], [27].
3) To derive general principles, we treat a weakly absorbing material with broadband single-pass absorption of 1.6%. This weak single-pass absorption reveals the full benefit of light trapping. Stronger absorbance would saturate the maximum AE possible, as seen in [15], [28]–[36].
4) We utilize a high-index absorber material with $n = 3.5$. Although [4], [5], and [37] exceed the ray optics limit for subwavelength absorber layers, they do so for a low-index absorber ($n < 2$) sandwiched by a higher index cladding.
5) In our optimization, we look for the most general optimal 3-D texture, rather than optimizing a 2-D texture (with no variation along the third dimension) [27], [38] or making constraints on the shape, such as optimizing 1-D or 2-D grating parameters [9], [15], [24], [32] or the arrangement of nanowires [16].

II. Optimization Algorithm

The optimization geometry is shown in Fig. 1, and is meant to be consistent with the practical requirements of a thin-film solar cell. The setup consists of a weakly absorbing semiconductor material of index $n = 3.5$, with average thickness of 100 nm, and a flat top surface that is compatible with a conventional antireflection (AR) coating. The unknown texture on the bottom surface is specified within 2-D periodic boundary conditions. The absorption is evaluated in the important solar frequency range, 350 THz to 400 THz (1.45 to 1.65 eV or 750 to 860 nm free space wavelength), a bandwidth relative to center frequency of 1/8. This is a bandedge photon energy range where even a direct bandgap semiconductor like GaAs needs some absorption assistance. We do not consider the full solar spectral bandwidth when designing a surface texture, since at most higher frequencies, the direct gap absorption is sufficient. Note that Maxwell's equations are scale invariant, meaning that solutions described here can be scaled to different bandgaps.

The average thickness of 100 nm is less than a half wavelength in the material, placing us in the subwavelength regime. An artificial weakly absorbing material ($n_{\mathrm{real}} = 3.5$ and $\alpha = 1.6 \times 10^3$ cm^{-1}) is chosen in order to arrive at general conclusions related to weak optical absorption. The semiconductor is specified to have a uniform $\alpha d = 0.016$ single-pass absorption throughout the band, small enough to benefit from light trapping, but large enough to allow faster numerical convergence and accuracy. A more highly absorbing material might saturate at 100% absorption, obscuring the benefit of the surface texturing.

An AR coating is applied to the top of the solar cell structure. It is fixed at a quarter wavelength (108 nm) for the center wavelength in the optimization bandwidth, with $n_{\mathrm{AR}} = \sqrt{(n_{\mathrm{air}} \times n_{\mathrm{absorber}})} = 1.85$. A bottom surface texture was chosen for the absorber layer so we can keep the AR coating fixed in our optimization algorithm. Beneath the absorber layer is a nonabsorbing back dielectric layer of $n = 1.5$ (adjusted to 133 nm average thickness) followed by a perfect back reflector.

The periodic surface texture function h is represented by a truncated Fourier series

$$h(x,y) = \sum_{m=-2,-1,0,1,2} \sum_{n=-2,-1,0,1,2} c_{mn} e^{i\frac{m2\pi x}{\Lambda_x}} e^{i\frac{n2\pi y}{\Lambda_y}} \quad (3)$$

where Λ_x and Λ_y are the periodicities in the x- and y-direction, respectively, and c_{mn} are the Fourier coefficients. In our optimization algorithm, we keep the periodicity and the zeroth-order Fourier coefficient (the average absorber layer thickness) fixed, and allow the other Fourier coefficients to evolve. We used a fixed square periodicity of 710 nm; this choice is the result of an optimization further explained in Section III. We truncate the Fourier series to avoid sharp corners and small highly resonant features that would not be robust in manufacturing (it should be noted that the corners in even a square wave fabricated by conventional top down lithography are not perfectly sharp).

Our optimization algorithm scripts are written in MATLAB, following the procedure described in [39]. Our optimization uses an adjoint gradient method to search for a local optimum [40]. To find the absorption of the solar cell, we simulate the solar cell structure of Fig. 1 in "Lumerical FDTD Solutions," a commercial finite-difference time-domain solver for Maxwell's equations, evaluating the absorption at 30 points within the frequency bandwidth. Each iteration takes approximately 15 min on our computational cluster of 128 cores, and the optimization converges after about 25 iterations. Although [38] similarly optimizes a truncated series of Fourier coefficients, they do so for a 2-D surface. The computational burden of optimizing in 3-D is much larger (both due to the increased number of Fourier coefficients and longer simulation time), thus we need to use the method described in [39] to efficiently compute the gradients of the geometric parameters with respect to the figure of merit.

The selection of the figure of merit is critical. We maximize the AE at the frequency with the lowest absorption, a minimax

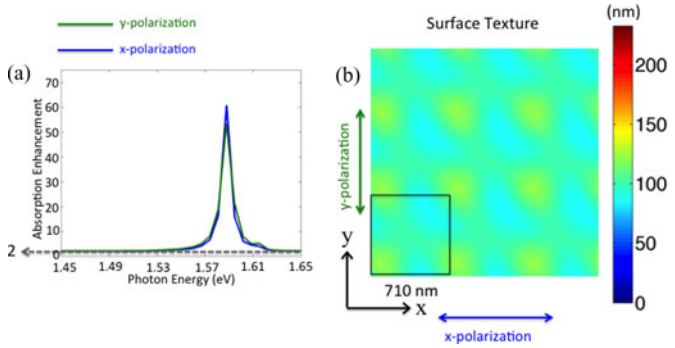

Fig. 2. (a) Initial AE as a function of frequency, at normal incidence and (b) top-down view of the surface texture; the colors show the height of the absorbing material (from the AR coating to the bottom dielectric, as seen in Fig. 1).

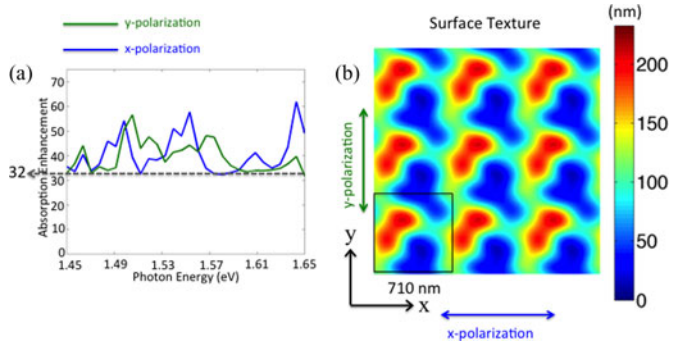

Fig. 3. (a) Final AE as a function of frequency, at normal incidence and (b) top-down view of the surface texture; the colors show the height of the absorbing material (from the AR coating to the bottom dielectric, as seen in Fig. 1).

figure of merit [41], which allows us to achieve good absorption over the whole frequency band. In one iteration, we evaluate the absorption for each frequency, at each of the two perpendicular polarizations of normally incident light. We then take the lowest AE as the figure of merit ($\mathrm{AE_{FOM}}$). At the end of the optimization, we compute the angle-averaged performance. The Lambertian angle-averaged enhancement ($\mathrm{AE_{angle}}$) as a function of frequency is given by

$$\mathrm{AE_{angle}} = \frac{\int_0^{2\pi}\int_0^{\frac{\pi}{2}} AE(\theta,\phi)\times\cos(\theta)\times\sin(\theta)d\theta d\phi}{\int_0^{2\pi}\int_0^{\frac{\pi}{2}} \cos(\theta)\times\sin(\theta)d\theta d\phi} \quad (4)$$

where AE is the absorption enhancement found by dividing the absorption by the average single-pass absorption $\alpha d = 0.016$, and averaging over the two perpendicular polarizations. At the end of the full optimization, we evaluate (4) by simulating 12 angles over the hemisphere, with two orthogonal polarizations for every angle.

III. Results and Discussion

We started the algorithm from noisy initial conditions with fixed square periodicity of 710 nm ($=3.1\lambda_{n=3.5}$, i.e., approximately three times the wavelength in the absorbing medium). We randomly picked initial Fourier coefficients in the range of 0–8 nm. In this first example, we achieved a minimum absorption enhancement $\mathrm{AE_{FOM}} = 32$ for a 100 nm average thickness absorber layer at normal incidence. The progression of the surface texture and AE at normal incidence from the first iteration to the last is shown in Figs. 2 and 3. The reciprocal space representation (the magnitudes and phases of the Fourier coefficients) of the final surface is shown in Fig. 4. The effect of our minimax figure of merit in optimizing for the lowest absorbing frequency and for achieving high absorption over the full band can be seen in this progression. Resonant peaks from the initial case flatten out, and both the minimum and average AE improve. The angle-averaged performance is shown in Fig. 5. Angle- and frequency-averaged, this texture achieves an absorption enhancement of $\mathrm{AE_{angle}} = 23$ relative to 1.6% single-pass absorption.

Our optimization algorithm is sensitive to initial conditions; Fig. 6 shows three cases of the final texture and final AE both at

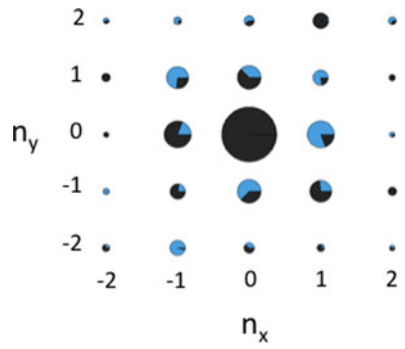

Fig. 4. Reciprocal (k-) space representation for the final texture seen in Fig. 3. The blue pie slices represent the phase of the complex exponential Fourier coefficients.

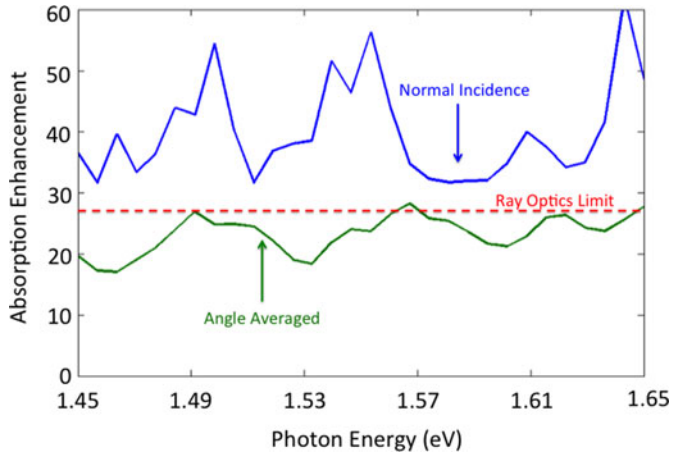

Fig. 5. Absorption enhancement (AE) for the texture in Fig. 3, plotted as a function of frequency at normal incidence, averaged over both polarizations, (blue) and angle averaged (green).

normal incidence and angle averaged for different initial conditions (randomly chosen initial Fourier coefficients in the range of 0–10 nm). Under different initial conditions, we obtain different textures reaching similar angle- and frequency-averaged absorption enhancements of $\mathrm{AE_{angle}} = 22$, 24, and 19. The best angle- and frequency-averaged absorption enhancement of $\mathrm{AE_{angle}} = 24$ is seen in the texture in Fig. 6(b); the AE for this texture as a function of incident angle is shown in Fig. 7. The

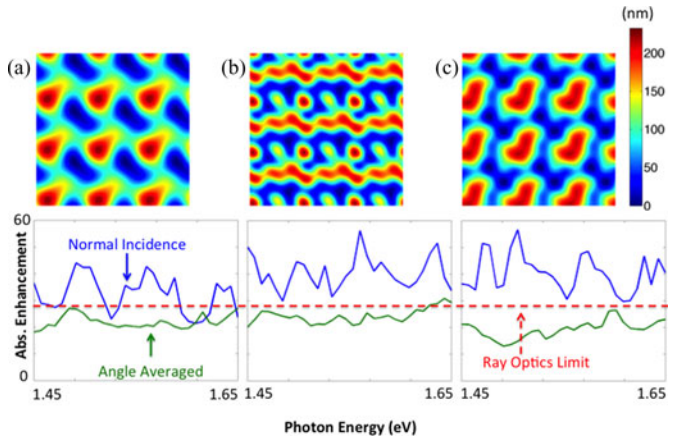

Fig. 6. Surface textures and AE as a function of frequency for different initial conditions, revealing a broad optimum.

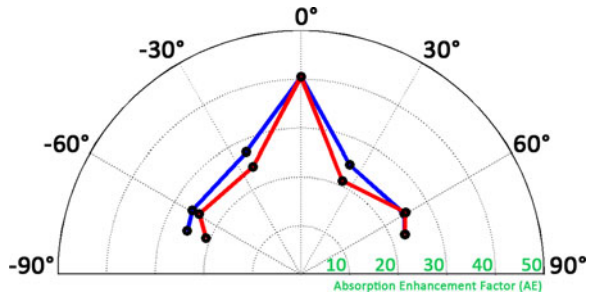

Fig. 7. Absorption enhancement factor (AE) averaged over frequency and polarization, as a function of incident angle θ in the x–z plane (blue) and the y–z plane (red).

TABLE I
FOURIER COEFFICIENTS (c_{mn}), IN NANOMETERS, APPLIED TO (3) THAT REPRESENT THE TEXTURE IN FIG. 6(b), THE OPTIMIZED TEXTURE WITH THE BEST ANGLE- AND FREQUENCY-AVERAGED AE ($\mathrm{AE_{angle}}$)

	m = -2	m = -1	m = 0	m = 1	m = 2
n = 2	1.25 + 2.75i	5.25 + 6i	9 - 17.5i	4.25 - 2.5i	3.25 - 11.75i
n = 1	8.5 - 2i	10 - 4.25i	-8.5 + 19i	-6 + 0.25i	-1 - 6.5i
n = 0	10 + 6.5i	8 - 1.5i	100	8 + 1.5i	10 - 6.5i
n = -1	-1 + 6.5i	-6 - 0.25i	-8.5 - 19i	10 + 4.25i	8.5 + 2i
n = -2	3.25 + 11.75i	4.25 + 2.5i	9 + 17.5i	5.25 - 6i	1.25 - 2.75i

Fourier coefficients (c_{mn}) for the texture in Fig. 6(b) are listed in Table I.

A common feature of the final optimized textures is large height amplitude. The full amplitudes for the textures in Figs. 3, 6(a), 6(b), and 6(c) are $\Delta h = 196$, 224, 218, and 217, respectively. The photonic bandstructure of the optimized texture from Fig. 6(b) is shown in Fig. 8. The optimization domain (the bandwidth of frequencies that we simulate) is highlighted in Fig. 8. The bandstructure visually shows the need for a high modal density in the optimization domain; the structure needs modes for the incident light to couple to.

The second common feature we observe is asymmetry within the unit cell. The optimal structures appear to break the inherent mirror symmetries of the problem, with a feature growing along one of the diagonals. To demonstrate that this symmetry breaking is not an artifact of the starting noise, we started another optimization from initial symmetrized conditions, with a slight

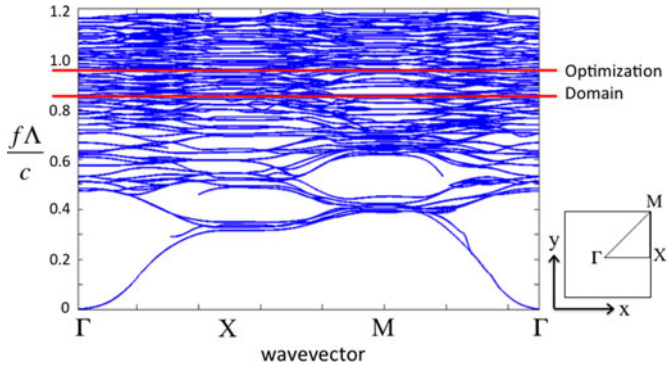

Fig. 8. Photonic bandstructure for the texture in Fig. 6(b).

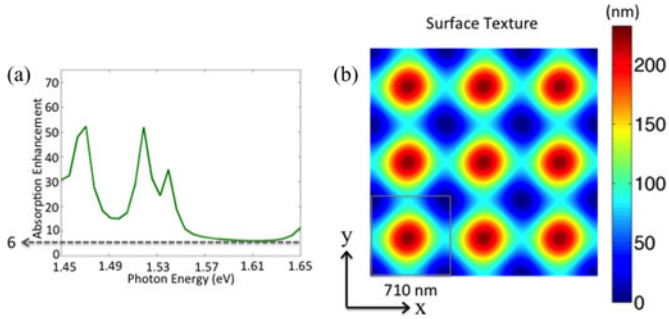

Fig. 9. (a) Initial AE as a function of frequency, at normal incidence and (b) top-down view of the surface texture, for a symmetric texture with a slight perturbation along the diagonal.

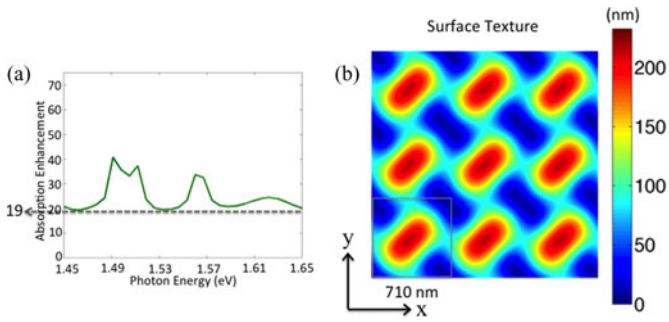

Fig. 10. (a) Final AE as a function of frequency, at normal incidence and (b) top-down view of the surface texture, showing broken mirror symmetry, from almost symmetric initial conditions seen in Fig. 9.

perturbation along the diagonal, as shown in Fig. 9. The result of the algorithm is shown 15 iterations later in Fig. 10 (reciprocal space diagram in Fig. 11). We see that this perturbation has been amplified along the diagonal, suggesting that symmetry breaking is a fundamental feature of optimal textures. There appears to be no significance to the direction of the asymmetric component: the symmetry will break in the opposite direction (along $x = -y$) if the initial perturbation is in that direction.

In our optimizations, we kept the periodicity fixed at 710 nm. To find the optimal periodicity, we ran a sweep of optimizations with fixed periodicities from 50 to 800 nm in increments of 50 nm. Fig. 12 plots $\mathrm{AE_{FOM}}$ (absorption enhancement at the minimum performing frequency at normal incidence) achieved in these optimizations. The smaller periodicities did not optimize well; periodicities less than 350 nm did not achieve

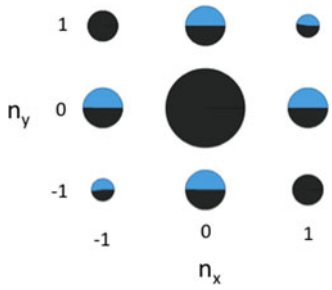

Fig. 11. Reciprocal space representation for the texture with broken mirror symmetry in Fig. 10. The blue pie slices represent the phase of the complex exponential Fourier coefficients.

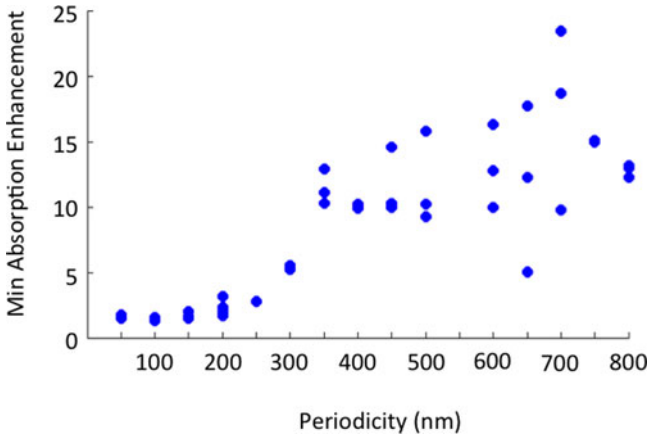

Fig. 12. Optimizations were carried out at periodicities from 50 to 800 nm, in increments of 50 nm. For each periodicity, at least three optimizations were completed for randomly chosen initial starting noise. The $\mathrm{AE_{FOM}}$ (absorption enhancement for the worst performing frequency and polarization at normal incidence) is plotted for each optimization.

minimum absorption enhancement $\mathrm{AE_{FOM}} > 10$. The best optimizations occurred at 700 nm; perhaps because this periodicity brought the optimization frequency band high into the photonic bandstructure where the optical density of states is large and allowed the optimal coupling to the internally propagating modes.

Since the optimum is not unique, it is possible that any randomly generated pattern with large amplitude could achieve a similar figure of merit ($\mathrm{AE_{FOM}}$). To check this, we randomly generated Fourier coefficients for 100 textures with a periodicity of 710 nm, with amplitudes ranging from $\Delta h = 223$ to 233 nm, and simulated the absorption of these structures. The $\mathrm{AE_{FOM}}$ (the lowest AE as a function of frequency at normal incidence, for the worst performing polarization) of these random structures are plotted in Fig. 13, and the random texture with the median figure of merit $\mathrm{AE_{FOM}} = 13$ is shown in Fig. 14. In Figs. 15 and 16, the random texture with the median $\mathrm{AE_{FOM}}$ is compared with the optimized texture shown in Fig. 6(b). The $\mathrm{AE_{FOM}}$ for the optimized texture is over two times greater than the median $\mathrm{AE_{FOM}}$ in the randomly generated patterns. A comparison of angle-averaged absorption performance (shown in Fig. 16) shows a 33% increase in the optimized texture's $\mathrm{AE_{angle}}$ over the $\mathrm{AE_{angle}}$ for the median randomly generated pattern.

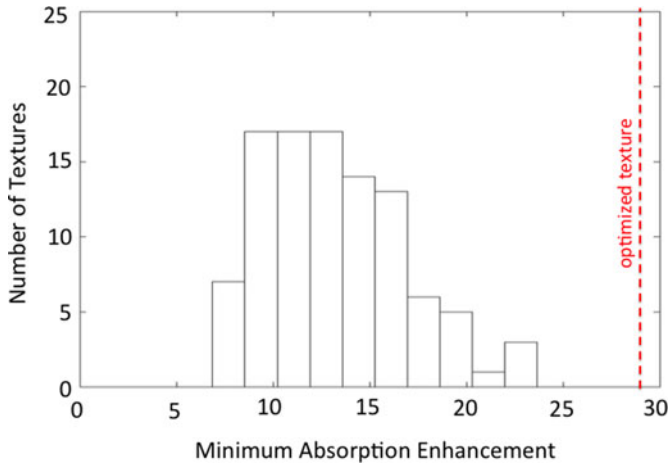

Fig. 13. $\mathrm{AE_{FOM}}$ (minimum absorption enhancement at normal incidence) plotted for 100 randomly generated textures of 710-nm periodicity. For comparison, the $\mathrm{AE_{FOM}}$ for the optimized texture in Fig. 6(b) is shown by the dotted red line.

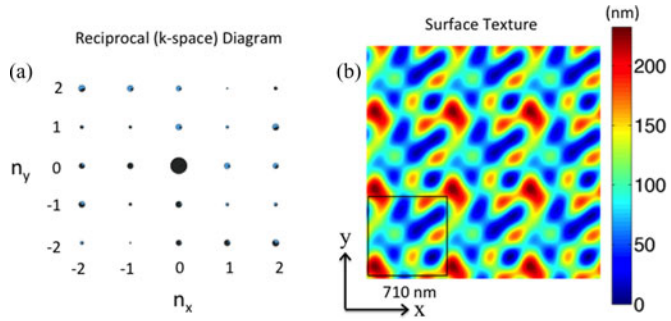

Fig. 14. (a) Reciprocal k-space diagram and (b) real-space top-down view of the median randomly generated texture from Fig. 13.

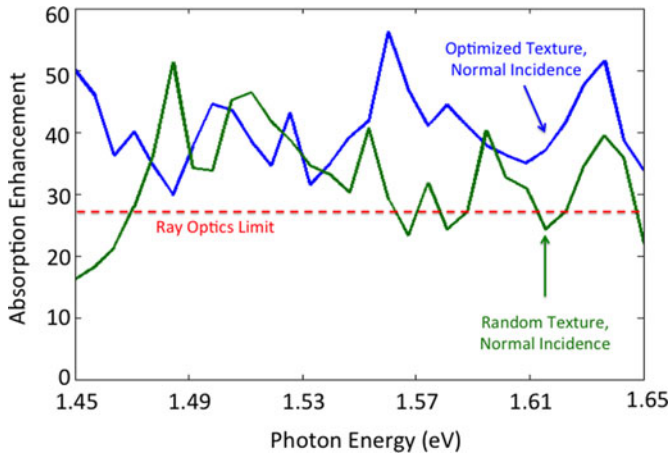

Fig. 15. Absorption enhancement (AE) as a function of frequency at normal incidence for the optimized texture from Fig. 6(b) (blue) compared with the median random texture from Fig. 14 (green). Lines are averaged over the two orthogonal polarizations.

We also check the performance of a completely random texture (i.e., a texture with infinite periodicity). We randomly generated Fourier coefficients to the fifth order for a periodicity that

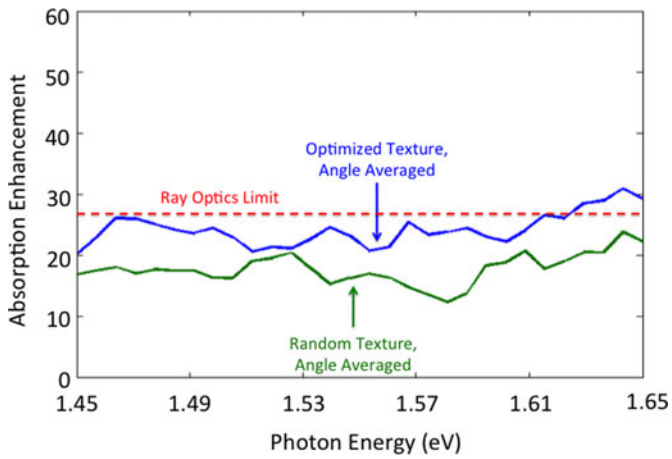

Fig. 16. Absorption enhancement (AE) as a function of frequency, angle averaged, for the optimized texture from Fig. 6(b) (blue) compared with the median random texture from Fig. 14 (green).

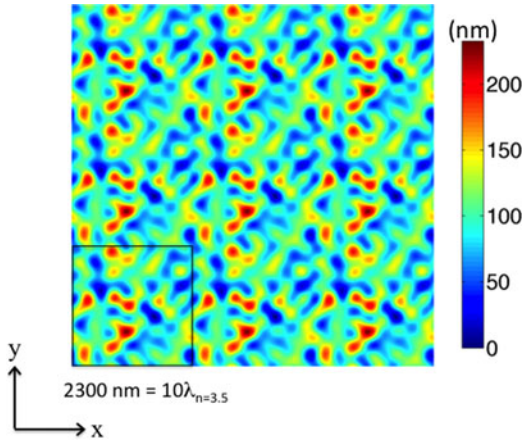

Fig. 18: A top-down view of the surface texture, for the randomly generated texture with periodicity of 2300 nm $= 10\lambda_{n=3.5}$, with median $\mathrm{AE_{FOM}}$ (minimum absorption enhancement at normal incidence).

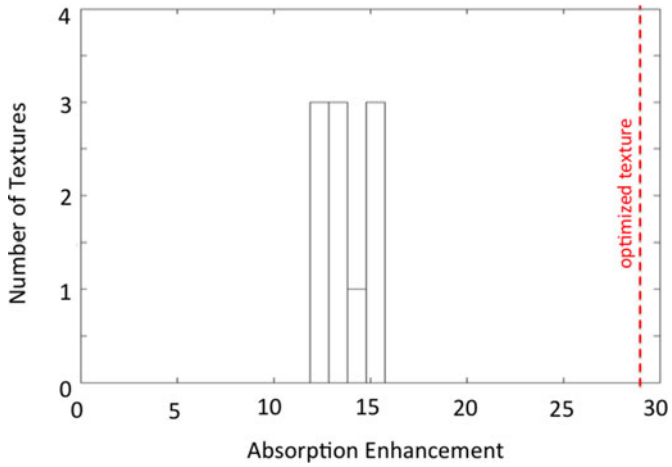

Fig. 17. $\mathrm{AE_{FOM}}$ (minimum absorption enhancement at normal incidence) plotted for 11 randomly generated textures of 2300-nm periodicity. For comparison, the $\mathrm{AE_{FOM}}$ for the optimized texture in Fig. 6(b) is shown by the dotted red line.

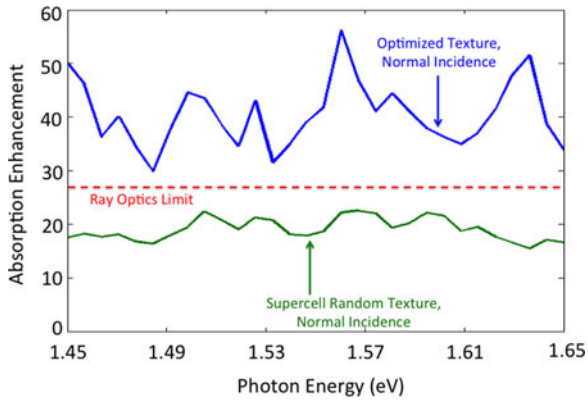

Fig. 19. Absorption enhancement (AE) as a function of frequency at normal incidence for the optimized texture from Fig. 6(b) (blue) compared with the median random texture with 2300-nm periodicity from Fig. 18 (green). Lines are averaged over the two orthogonal polarizations.

is $10\lambda_{n=3.5} = 2300$ nm, with a total texture amplitude between $\Delta h = 223$ nm and 233 nm. Our large periodicity approximates a texture with infinite periodicity (the supercell approach). The resulting $\mathrm{AE_{FOM}}$ for 11 different random supercell textures is shown in Fig. 17. The texture with the median figure of merit of $\mathrm{AE_{FOM}} = 13$ is shown in Fig. 18; this median $\mathrm{AE_{FOM}}$ is the same as for the random textures on a 710-nm periodicity. Fig. 19 compares the median supercell texture with the optimized texture at normal incidence. Additionally, the angle- and frequency-averaged performance (see Fig. 20) of the optimized texture is 26% better than the median random supercell. Our result that a periodic texture can perform better than a random one in the subwavelength regime is in agreement with [42].

In Table II, AE relative to 1.6% single-pass absorption is summarized. To compare these results with the $4n^2$ ray-optics AE limit, we need to account for the finite absorption in our structure. This can be done by using (1), which can be written

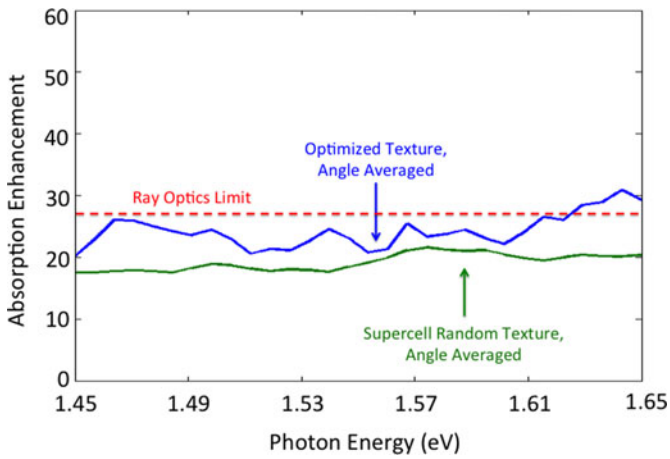

Fig. 20. Absorption enhancement (AE) as a function of frequency, angle averaged, for the optimized texture from Fig. 6(b) (blue) compared with the median random texture with 2300-nm periodicity from Fig. 18 (green).

TABLE II
SUMMARY OF AES AND WEAK ABSORPTION LIMIT ENHANCEMENTS (E)

	Best Optimized Texture	Median Random Texture (710 nm periodicity)	Median Random Supercell Texture (2300 nm periodicity)	Ray Optics Limit
AE_{FOM} (worst enhancement factor over frequency and polarization at normal incidence)	29	13	13	
AE_{angle} (angle- and frequency-averaged enhancement factor)	24	18	19	27
E (enhancement factor in the weakly absorbing limit)	39	25	27	49

more generally as

$$A = \frac{\alpha d}{\alpha d + \frac{1}{4n^2}} = \frac{\alpha d}{\alpha d + \frac{1}{E}} \tag{5}$$

where E is the limiting enhancement factor when the single-pass absorption is very weak ($\alpha d < 1.6\%$). E represents the highest possible enhancement factor, which should be compared with the ray-optics ideal $E = 4n^2 \sim 50$ case. For our optimized case of $\mathrm{AE}_{\mathrm{angle}} = 24$ at $\alpha d = 0.016$, $E = 39$. Our AE and weak absorption limit (E) results are summarized in Table II.

IV. CONCLUSION

In the ray optics regime, random structures are optimal to achieve AE [1]. In the subwavelength regime, it appears that computationally optimized surface textures perform better than randomly generated ones. So far, we have discovered a broad optimum, with many textures that achieve similar figures of merit. We have shown that our optimized structures perform about 33% better than randomly generated structures for angle- and frequency-averaged absorption. We report an angle- and frequency-averaged AE factor in the weakly absorbing limit of $E = 39$, for a texture on a high-index material of subwavelength thickness. This enhancement is $\sim$80% of the ray optics limit $E = 4n^2 \sim 50$.

Although we do not prove a fundamental limit, the AE factor that arises from these optimizations is less than the ray-optics limit. It should be noted that for practical purposes, meeting or exceeding the ray-optics limit in the subwavelength might be unnecessary. For example, starting from a 1-μm film thickness, which for some materials makes a good solar cell even without light trapping, an enhancement factor $E = 50$ would permit a reduced film thickness $<$100 nm.

In evaluating the performance of a solar cell texture for light trapping, it is important to take into account both the average performance, as well as the worst performance over the frequency. A texture with a few resonant peaks may yield high average performance in theory, but when applied to a real material, the resonant peaks will saturate at 100% absorption, and the total photons absorbed will be low. This electromagnetic optimization procedure obtains both a broadband absorption spectrum and a high average absorption.

Our practical goal in designing a solar cell texture is to achieve complete light absorption in the thinnest possible layer, with a manufacturable texture. This study is meant to be a general discussion of light trapping in the subwavelength thickness regime, and not specific to a certain material. However, this optimization procedure can be used as a tool in designing textures for real materials. Future work also requires the optimization of the AR coating. The one-layer AR coating only works for normal incidence at the center of the chosen frequency band. In reality, the AR coating needs to have good angle-averaged performance, especially for the large energy photons outside the optimized bandwidth. In addition, many authors [43] have attempted to use metal nanostructures to enhance solar cell absorption. Some problems with this approach include parasitic absorption in the metals and shadowing losses. In future work, metal nanostructures can also be included in the optimization of the light trapping structure. Furthermore, we can add manufacturing constraints to the problem. For example, in these calculations, we permitted the minimum film thickness to drop as low as 1 nm, but we could constrain to a more realistic minimum thickness of 50 nm. Finally, in our procedure, we could have fallen into local optima and not found the global optimum. Further work requires us to investigate the question of whether we have really converged.

REFERENCES

[1] E. Yablonovitch, "Statistical ray optics," *J. Opt. Soc. Amer.*, vol. 72, no. 7, pp. 899–907, Jul. 1982.
[2] O. D. Miller, E. Yablonovitch, and S. R. Kurtz, "Strong internal and external luminescence as solar cells approach the Shockley-Queisser limit," *IEEE J. Photovolt.*, vol. 2, no. 3, pp. 303–311, Jul. 2012.
[3] G. Lush and M. Lundstrom, "Thin film approaches for high-efficiency III–V cells," *Sol. Cells*, vol. 30, no. 1–4, pp. 337–344, May 1991.
[4] M. A. Green, "Enhanced evanescent mode light trapping in organic solar cells and other low index optoelectronic devices," *Prog. Photovolt., Res. Appl.*, vol. 19, no. 4, pp. 473–477, Jun. 2011.
[5] Z. Yu, A. Raman, and S. Fan, "Fundamental limit of nanophotonic light trapping in solar cells," *Proc. Nat. Acad. Sci.*, vol. 107, no. 41, pp. 17491–17496, Sep. 2010.
[6] H. R. Stuart and D. G. Hall, "Thermodynamic limit to light trapping in thin planar structures," *J. Opt. Soc. Amer. A*, vol. 14, no. 11, pp. 3001–3008, Nov. 1997.
[7] Z. Yu and S. Fan, "Angular constraint on light-trapping absorption enhancement in solar cells," *Appl. Phys. Lett.*, vol. 98, no. 1, pp. 011106-1–011106-3, 2011.
[8] Z. Yu, A. Raman, and S. Fan, "Thermodynamic upper bound on broadband light coupling with photonic structures," *Phys. Rev. Lett.*, vol. 109, no. 17, pp. 173901-1–173901-5, Oct. 2012.
[9] Z. Yu, A. Raman, and S. Fan, "Fundamental limit of light trapping in grating structures," *Opt. Exp.*, vol. 18, no. S3, pp. A366–A380, Aug. 2010.
[10] L. Zeng, Y. Yi, C. Hong, J. Liu, N. Feng, X. Duan, L. C. Kimerling, and B. A. Alamariu, "Efficiency enhancement in Si solar cells by textured photonic crystal back reflector," *Appl. Phys. Lett.*, vol. 89, no. 11, pp. 111111-1–111111-3, 2006.
[11] E. Garnett and P. Yang, "Light trapping in silicon nanowire solar cells," *Nano Lett.*, vol. 10, no. 3, pp. 1082–1087, Mar. 2010.
[12] D. Shir, J. Yoon, D. Chanda, J.-H. Ryu, and J. A. Rogers, "Performance of ultrathin silicon solar microcells with nanostructures of relief formed by soft imprint lithography for broad band absorption enhancement," *Nano Lett.*, vol. 10, no. 8, pp. 3041–3046, Aug. 2010.
[13] P. Bermel, C. Luo, L. Zeng, L. C. Kimerling, and J. D. Joannopoulos, "Improving thin-film crystalline silicon solar cell efficiencies with photonic crystals," *Opt. Exp.*, vol. 15, no. 25, pp. 16986–17000, 2007.
[14] C. Heine and R. H. Morf, "Submicrometer gratings for solar energy applications," *Appl. Opt.*, vol. 34, no. 14, pp. 2476–2482, May 1995.

[15] N. Senoussaoui, M. Krause, J. Müller, E. Bunte, T. Brammer, and H. Stiebig, "Thin-film solar cells with periodic grating coupler," *Thin Solid Films*, vol. 451/452, pp. 397–401, Mar. 2004.
[16] M. D. Kelzenberg, S. W. Boettcher, J. A. Petykiewicz, D. B. Turner-Evans, M. C. Putnam, E. L. Warren, J. M. Spurgeon, R. M. Briggs, N. S. Lewis, and H. A. Atwater, "Enhanced absorption and carrier collection in Si wire arrays for photovoltaic applications," *Nature Mater.*, vol. 9, pp. 239–244, Feb. 2010.
[17] K. X. Wang, Z. Yu, V. Liu, Y. Cui, and S. Fan, "Absorption enhancement in ultrathin crystalline silicon solar cells with antireflection and light-trapping nanocone gratings," *Nano Lett.*, vol. 12, no. 3, pp. 1616–1619, Mar. 2012.
[18] D. Madzharov, R. Dewan, and D. Knipp, "Influence of front and back grating on light trapping in microcrystalline thin-film silicon solar cells," *Opt. Exp.*, vol. 19, no. S2, pp. A95–A107, Jan. 2011.
[19] P. Kowalczewski, M. Liscidini, and L. C. Andreani, "Engineering Gaussian disorder at rough interfaces for light trapping in thin-film solar cells," *Opt. Lett.*, vol. 37, no. 23, pp. 4868–4870, Nov. 2012.
[20] S. Eyderman, S. John, and A. Deinega, "Solar light trapping in slanted conical-pore photonic crystals: Beyond statistical ray trapping," *J. Appl. Phys.*, vol. 113, no. 15, pp. 154315-1–154315-10, 2013.
[21] I. Tobías, A. Luque, and A. Martí, "Light intensity enhancement by diffracting structures in solar cells," *J. Appl. Phys.*, vol. 104, no. 3, pp. 034502-1–034502-10, 2008.
[22] C. Wang, S. Yu, W. Chen, and C. Sun, "Highly efficient light-trapping structure design inspired by natural evolution," *Sci. Rep.*, vol. 3, Jan. 2013.
[23] E. R. Martins, J. Li, Y. Liu, J. Zhou, and T. F. Krauss, "Engineering gratings for light trapping in photovoltaics: The supercell concept," *Phys. Rev. B*, vol. 86, no. 4, pp. 041404-1–041404-4, Jul. 2012.
[24] A. Abass, K. Q. Le, A. Alù, M. Burgelman, and B. Maes, "Dual-interface gratings for broadband absorption enhancement in thin-film solar cells," *Phys. Rev. B*, vol. 85, no. 11, pp. 115449-1–115449-8, Mar. 2012.
[25] Z. Xia, Y. Wu, R. Liu, Z. Liang, J. Zhou, and P. Tang, "Misaligned conformal gratings enhanced light trapping in thin film silicon solar cells," *Opt. Exp.*, vol. 21, no. S3, pp. A548–A557, May 2013.
[26] P. Sheng, "Wavelength-selective absorption enhancement in thin-film solar cells," *Appl. Phys. Lett.*, vol. 43, no. 6, pp. 579-1–579-3, 1983.
[27] M. B. Dühring and O. Sigmund, "Optimization of extraordinary optical absorption in plasmonic and dielectric structures," *J. Opt. Soc. Amer. B*, vol. 30, no. 5, pp. 1154–1160, Apr. 2013.
[28] J. Zhu, C.-M. Hsu, Z. Yu, S. Fan, and Y. Cui, "Nanodome solar cells with efficient light management and self-cleaning," *Nano Lett.*, vol. 10, no. 6, pp. 1979–1984, Jun. 2010.
[29] P. N. Saeta, V. E. Ferry, D. Pacifici, J. N. Munday, and H. A. Atwater, "How much can guided modes enhance absorption in thin solar cells?" *Opt. Exp.*, vol. 17, no. 23, pp. 20975–20990, Nov. 2009.
[30] D. Zhou and R. Biswas, "Photonic crystal enhanced light-trapping in thin film solar cells," *J. Appl. Phys.*, vol. 103, no. 9, pp. 093102-1–093102-5, 2008.
[31] Y. Park, E. Drouard, O. El Daif, X. Letartre, P. Viktorovitch, A. Fave, A. Kaminski, M. Lemiti, and C. Seassal, "Absorption enhancement using photonic crystals for silicon thin film solar cells," *Opt. Exp.*, vol. 17, no. 16, pp. 14312–14321, Jul. 2009.
[32] C. Eisele, C. E. Nebel, and M. Stutzmann, "Periodic light coupler gratings in amorphous thin film solar cells," *J. Appl. Phys.*, vol. 89, no. 12, pp. 7722-1–7722-5, 2001.
[33] V. E. Ferry, M. A. Verschuuren, H. B. T. Li, E. Verhagen, R. J. Walters, R. E. I. Schropp, H. A. Atwater, and A. Polman, "Light trapping in ultrathin plasmonic solar cells," *Opt. Exp.*, vol. 18, no. S2, pp. A237–A245, Jun. 2010.
[34] S. Fahr, T. Kirchartz, C. Rockstuhl, and F. Lederer, "Approaching the Lambertian limit in randomly textured thin-film solar cells," *Opt. Exp.*, vol. 19, no. S4, pp. A865–A874, Jun. 2011.
[35] J. Grandidier, D. M. Callahan, J. N. Munday, and H. A. Atwater, "Light absorption enhancement in thin-film solar cells using whispering gallery modes in dielectric nanospheres," *Adv. Mater.*, vol. 23, no. 10, pp. 1272–1276, Mar. 2011.
[36] F. Pratesi, M. Burresi, F. Riboli, K. Vynck, and D. S. Wiersma, "Disordered photonic structures for light harvesting in solar cells," *Opt. Exp.*, vol. 21, no. S3, pp. A460–A468, Apr. 2013.
[37] D. M. Callahan, J. N. Munday, and H. A. Atwater, "Solar cell light trapping beyond the ray optic limit," *Nano Letters*, vol. 12, no. 1, pp. 214–218, Jan. 2012.
[38] X. Sheng, S. G. Johnson, J. Michel, and L. C. Kimerling, "Optimization-based design of surface textures for thin-film Si solar cells," *Opt. Exp.*, vol. 19, no. S4, pp. A841–A850, Jun. 2011.
[39] O. Miller, "Photonic design: From fundamental solar cell physics to computational inverse design," Ph.D. dissertation, EECS Dept., Univ. California, Berkeley, CA, USA, 2012.
[40] M. B. Giles and N. A. Pierce, "An introduction to the adjoint approach to design," *Flow, Turbul. Combust.*, vol. 65, no. 3–4, pp. 393–415, Jan. 2000.
[41] W. Murray and M. L. Overton, "A projected Lagrangian algorithm for nonlinear minimax optimization," *SIAM J. Sci. Stat. Comput.*, vol. 1, no. 3, pp. 345–370, Sep. 1980.
[42] C. Battaglia, C.-M. Hsu, K. Söderström, J. Escarré, F.-J. Haug, M. Charrière, M. Boccard, M. Despeisse, D. T. L. Alexander, M. Cantoni, Y. Cui, and C. Ballif, "Light trapping in solar cells: Can periodic beat random?" *ACS Nano*, vol. 6, no. 3, pp. 2790–2797, Mar. 2012.
[43] V. E. Ferry, J. N. Munday, and H. A. Atwater, "Design considerations for plasmonic photovoltaics," *Adv. Mater.*, vol. 22, no. 43, pp. 4794–4808, Nov. 2010.

Authors' photographs and biographies not available at the time of publication.